

Beyond Superficial Unlearning: Sharpness-Aware Robust Erasure of Hallucinations in Multimodal LLMs

Xianya Fang^{♣*}, Feiyang Ren^{♣*}, Xiang Chen^{♣†}, Yu Tian[♣],
Zhen Bi[◇], Haiyang Yu^{♡■}, Sheng-Jun Huang[♣]

[♣]Nanjing University of Aeronautics and Astronautics

[♣]Institute for AI, Tsinghua University [◇]Huzhou University

[♡]Institute of Dataspace, Hefei Comprehensive National Science Center

[■]University of Science and Technology of China

{xyfang, xiang_chen}@nuaa.edu.cn

Abstract

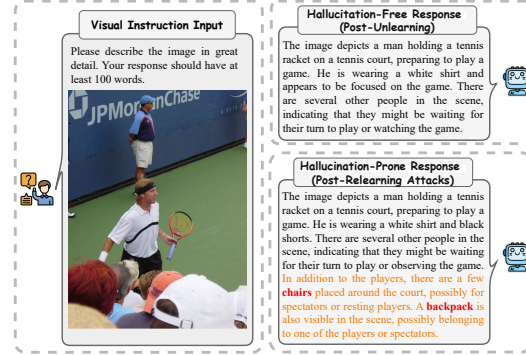
Multimodal LLMs are powerful but prone to object hallucinations, which describe non-existent entities and harm reliability. While recent unlearning methods attempt to mitigate this, we identify a critical flaw: structural fragility. We empirically demonstrate that standard erasure achieves only superficial suppression, trapping the model in sharp minima where hallucinations catastrophically resurge after lightweight relearning. To ensure geometric stability, we propose SARE, which casts unlearning as a targeted min–max optimization problem and uses a Targeted-SAM mechanism to explicitly flatten the loss landscape around hallucinated concepts. By suppressing hallucinations under simulated worst-case parameter perturbations, our framework ensures robust removal stable against weight shifts. Extensive experiments demonstrate that SARE significantly outperforms baselines in erasure efficacy while preserving general generation quality. Crucially, it maintains persistent hallucination suppression against relearning and parameter updates, validating the effectiveness of geometric stabilization.

1 Introduction

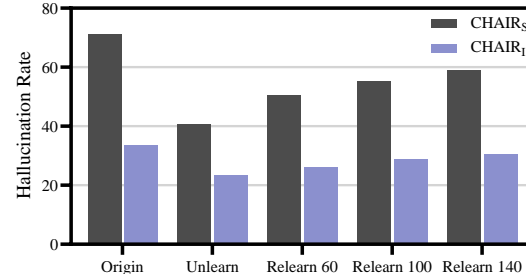
Multimodal Large Language Models (MLLMs) have reshaped the landscape of vision-language tasks, demonstrating exceptional proficiency in image captioning (Lai et al., 2024; Li et al., 2023a; Wang et al., 2022a) and visual question answering (Singh et al., 2024; Ji et al., 2022). However, this prowess is shadowed by the persistent issue of hallucination (Liu et al., 2024a; Chen et al., 2023c; Biten et al., 2021; Li et al., 2023c), where generated text conflicts with visual evidence. Such unfaithful outputs fundamentally undermine the

* Equal Contribution.

† Corresponding Author.



(a) Vulnerability of existing unlearning methods in MLLMs



(b) Hallucination Rates under Relearning

Figure 1: The vulnerability of unlearned MLLMs against relearning attacks. (a) Lightweight relearning can easily reactivate suppressed hallucinations. (b) The hallucination rate of EFUF exhibits a rapid resurgence as the number of relearning samples increases.

trustworthiness of MLLMs in real-world applications, necessitating effective mitigation strategies.

Existing countermeasures typically fall into two categories: *training-stage alignment* (Gunjal et al., 2023; Sun et al., 2023; Yu et al., 2023a; Zhao et al., 2024) and *inference-stage intervention* (Yin et al., 2023; Wang et al., 2023a; Chen et al., 2023a). While effective, the former incurs prohibitive data annotation and retraining costs, whereas the latter often imposes significant inference latency. Consequently, **machine unlearning** has emerged as a compelling, resource-efficient paradigm (Cao and

Yang, 2015; Ullah et al., 2021). By selectively "forgetting" specific hallucination patterns without full retraining, methods like EFUF (Xing et al., 2024) promise a balance between efficiency and safety.

However, we argue that current unlearning approaches for MLLMs remain *superficial*. Our empirical analysis reveals a startling fragility: models subjected to standard unlearning exhibit a rapid resurgence of hallucinations when subjected to relearning attacks (Lynch et al., 2024; Deeb and Roger, 2024), which involves exposure to a negligible amount of the original hallucination-inducing data. As shown in Figure 1a, unlearned models initially produce hallucination-free captions, but quickly revert to hallucination-prone behaviour after only tens of relearning samples. Quantitatively, Figure 1b shows that EFUF's hallucination rate rises sharply with more relearning samples, regressing to the pre-unlearning baseline.

From an optimization perspective, we hypothesize that standard unlearning procedures tend to push model parameters into a *sharp minimum* of the hallucination loss landscape. In such a precarious configuration, hallucination suppression is highly sensitive: even minor parameter changes, such as those introduced by relearning, can quickly move the model back into a hallucination-prone region. In other words, the unwanted knowledge is not truly erased but only suppressed at a sharp local basin, leaving the model vulnerable to regression under subsequent training.

To address this, we propose Sharpness-Aware Robust Erasure of Hallucinations in Multimodal LLMs (**SARE**), a novel framework that enforces robust erasure through geometric regularization. Drawing inspiration from Sharpness-Aware Minimization (SAM) (Foret et al., 2020a), **SARE** reformulates the unlearning objective as a targeted min-max problem. Instead of simply minimizing the unlearning loss, **SARE** simulates a worst-case attack by identifying the weight perturbation most likely to reactivate hallucinations, and minimizes the loss under this adversarial condition. This process effectively flattens the loss landscape around the unlearned state, ensuring that the erasure of hallucinations is stable and invariant to small weight shifts. Crucially, **SARE** retains the data-efficient curation pipeline of existing methods while fundamentally upgrading the optimization mechanism. Our contributions are summarized as follows:

- To the best of our knowledge, we are the first

to reveal the robustness gap in MLLM hallucination unlearning, collapsing rapidly under lightweight relearning attacks.

- We introduce **SARE**, a sharpness-aware framework optimizing for flat minima via Targeted-SAM to ensure deep, durable hallucination erasure while preserving general capabilities.
- **SARE** achieves persistent hallucination erasure that resists regression. Extensive experiments verify its stability against relearning, fine-tuning, and adversarial prompting.

2 Related Work

2.1 Hallucination Mitigation of MLLMs

Hallucination in MLLMs (Zhu et al., 2024; Li et al., 2023b) refers to cross-modal misalignment where textual outputs contradict visual evidence (Liu et al., 2024a; Chen et al., 2023c). The most prevalent and detrimental subtype is object hallucination, which describes non-existent items (Biten et al., 2021; Liu et al., 2024a; Li et al., 2023c). Addressing this issue is critical as it severely impairs model reliability in real-world applications (Wang et al., 2022b; Zhao et al., 2023; Huang et al., 2023; Zhang et al., 2023).

Existing mitigation strategies for MLLMs can be categorized into training-stage and inference-stage methods. Training-stage methods, such as fine-tuning on specialized datasets (You et al., 2023; Gunjal et al., 2023) or applying advanced alignment objectives like RLHF (Sun et al., 2023; Yu et al., 2023a; Zhao et al., 2024), improve alignment but demand expensive data and retraining costs. Inference-stage methods, including post-hoc revision (Yin et al., 2023) and training-free decoding (Wang et al., 2023a; Chen et al., 2023a; Ji et al., 2022), bypass retraining but increase latency and complexity (Yu et al., 2023a). Therefore, a resource-efficient approach that fundamentally mitigates hallucinations is critically needed.

2.2 Unlearning and Its Adversarial Robustness in LLMs

Machine unlearning refers to a technique designed to enable models to selectively erase specific data or behaviors while preserving general utility, serving as an efficient alternative to full retraining (Cao and Yang, 2015; Ullah et al., 2021). Common unlearning techniques primarily employ methods like gradient ascent (Jang et al., 2022a) or

KL-divergence constraints to balance these objectives (Yu et al., 2023a). However, existing methods are vulnerable to adversarial attacks. Of particular concern are relearning attacks, where fine-tuning the unlearned model with even a small amount of the original “forgotten” data can rapidly restore the undesired knowledge and behaviors (Lynch et al., 2024; Deeb and Roger, 2024). Pioneering work like EFUF has introduced unlearning to multimodal hallucination mitigation, but inherits these robustness limitations. In our research, we address this by developing a robust unlearning framework for MLLMs to defend against such attacks.

2.3 Sharpness Awareness Minimization

Sharpness-Aware Minimization (SAM) enhances model generalization by guiding the training towards parameters lying in neighborhoods with uniformly low loss, thereby promoting a flat loss landscape (Foret et al., 2020b). Formulated as a min-max optimization problem, SAM and its variants (e.g., ASAM (Kwon et al., 2021), ESAM (Du et al., 2021)) explicitly pursue flat minima to improve generalization (Bartlett et al., 2022; Ujv’ary et al., 2022). Beyond generalization, this smoothness is linked to robustness: SAM’s mechanism of optimizing against worst-case parameter perturbations has proven effective in adversarial training to defend against input-level attacks (Wei et al., 2023; Liu et al., 2024b). Recent theoretical insights further reveal a duality between SAM and Adversarial Training (AT) and demonstrate that SAM learns more robust feature representations (Zhang et al., 2024b). Motivated by these principles, we integrate SAM’s smoothness optimization to develop a robust unlearning framework for MLLMs specifically designed to withstand relearning attacks.

3 Methodology

3.1 Why Standard Unlearning Fails to Erase Hallucinations?

Standard unlearning typically employs a multi-objective optimization strategy: minimizing the likelihood of hallucinated samples while maintaining performance on normal data. Formally, the baseline objective is defined as:

$$\mathcal{L}_{base}(\theta_\phi) = \mathcal{L}_{pos} + \lambda_1 \mathcal{L}_{neg} + \lambda_2 \mathcal{L}_{sent}, \quad (1)$$

where \mathcal{L}_{neg} suppresses spurious hallucination correlations, while \mathcal{L}_{pos} and \mathcal{L}_{sent} preserve visual grounding and linguistic capabilities.

However, directly minimizing \mathcal{L}_{base} traps the model in a *sharp minimum*. As shown in Figure 1, this geometric characteristic implies extreme sensitivity to parameter changes: while the model successfully suppresses hallucinations at the exact optimal weights, adding even a slight perturbation causes the hallucination rate to spike drastically. This indicates that the erasure is structurally fragile, the unlearning effect is strictly confined to a precise point and cannot withstand the weight shifts inherent in model deployment or subsequent tuning. To bridge this gap, we draw inspiration from the adversary-defense game perspective (Fan et al., 2025). We hypothesize that true hallucination mitigation demands geometric stability—a flat loss landscape where the erasure remains effective even when parameters drift. Thus, we frame unlearning as a targeted min-max robust optimization problem.

3.2 SARE: A Framework for Robust Hallucination Erasure

Based on these insights, we propose **SARE**, a robust unlearning framework designed to harmonize data efficiency with optimization stability. As illustrated in Figure 2, our approach unfolds in two stages: The first stage is **Data Curation for Hallucination Unlearning**. We adopt an automated pipeline established by EFUF (Xing et al., 2024) to curate subsets: the negative subsentence dataset (D_{neg}) containing object hallucinations for erasure, the positive subsentence dataset (D_{pos}) for retaining visual grounding, and the sentence-level dataset (D_{sent}) to preserve linguistic coherence.

The second stage is **Targeted Sharpness Tuning**. To address the vulnerability of sharp minimum, we implement a Targeted-SAM mechanism. Rather than standard gradient descent, we first simulate a worst-case attack by maximizing the likelihood of hallucination relapse on D_{neg} , and then minimize the joint objective to suppress hallucinations and preserve capabilities on D_{pos} and D_{sent} under this worst-case interference. This enforces a flat loss landscape, ensuring that the erasure of hallucinations remains stable against weight shifts.

3.3 Data Curation for Hallucination Unlearning

To circumvent the prohibitive costs of manual annotation, we directly leverage the automated data curation pipeline established by EFUF (Xing et al., 2024). We employ CLIP-based alignment scores as a reliable proxy for visual grounding: high scores

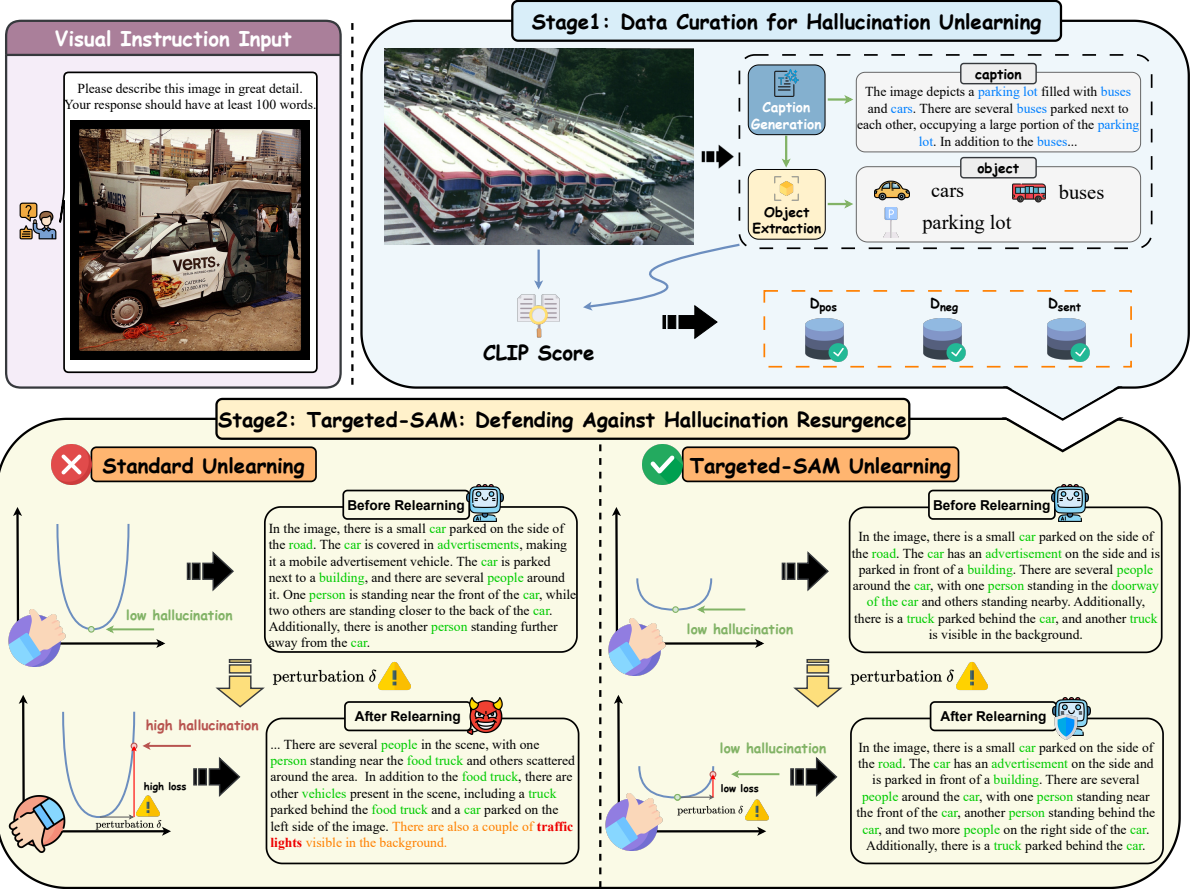


Figure 2: Overview of the **SARE** framework. The top-right panel illustrates Stage 1, where an automated pipeline curates training subsets (D_{neg} , D_{pos} , D_{sent}). The bottom panel depicts Stage 2, contrasting the fragile sharp minima of standard unlearning (left) with the robust flat loss landscape of **SARE** (right).

indicate accurately recognized objects, while low scores identify hallucinated content. Formally, for each object o identified in a response, the training unit is denoted as $u_o = (v, \text{pre}(o), \text{cur}(o))$, where v is the visual input, $\text{cur}(o)$ is the subsentence describing object o , and $\text{pre}(o)$ captures the preceding context. We adopt EFUF’s determined thresholds T_0 for high-confidence grounding and T_1 for hallucinated content to categorize object scores $S(o)$ into visual anchors (D_{pos}) and targets (D_{neg}):

$$\begin{aligned} D_{pos} &= \{u_o \mid S(o) > T_0\}, \\ D_{neg} &= \{u_o \mid S(o) < T_1\}. \end{aligned} \quad (2)$$

Additionally, to prevent the unlearning process from degrading the model’s fluency or instruction-following abilities, we utilize the sentence-level dataset D_{sent} , obtained by filtering responses with an average relevance score $S(y)$ above a sentence-level reliability threshold T_2 :

$$D_{sent} = \{(v, x, y) \mid S(y) > T_2\}, \quad (3)$$

comprising the image v , prompt x , and the reliable response y .

With these curated subsets, we explicitly define the loss components introduced in Sec. 3.1. Using the standard fine-tuning objective \mathcal{L}_{ft} , we minimize the loss on positive anchors and general instructions to preserve grounding, while inverting the loss on negative targets to penalize hallucination:

$$\begin{aligned} \mathcal{L}_{pos}(\theta_\phi) &= \mathcal{L}_{ft}(v, \text{pre}(o), \text{cur}(o)), \quad u_o \in D_{pos}, \\ \mathcal{L}_{neg}(\theta_\phi) &= -\mathcal{L}_{ft}(v, \text{pre}(o), \text{cur}(o)), \quad u_o \in D_{neg}, \\ \mathcal{L}_{sent}(\theta_\phi) &= \mathcal{L}_{ft}(v, x, y), \quad (v, x, y) \in D_{sent}. \end{aligned} \quad (4)$$

These objectives provide the foundational signals for our subsequent Targeted-SAM.

3.4 Targeted-SAM: Defending Against Hallucination Resurgence

Min-Max Formulation and Sharpness Regularization. Formulating the robust unlearning pro-

cess as a min-max problem, we design a targeted adversarial attack to simulate the worst-case scenario where hallucinations are most likely to resurface. Specifically, the inner maximization seeks a parameter perturbation ϵ that maximizes the probability of generating hallucinated objects (\mathcal{L}_{neg}), effectively exposing the model’s most vulnerable geometric direction. The outer minimization then suppresses hallucinations under this worst-case interference while anchoring valid capabilities on the original weights:

$$\min_{\theta_\phi} \left(\underbrace{\max_{\|\epsilon\|_2 \leq \rho} \lambda_1 \mathcal{L}_{neg}(\theta_\phi + \epsilon)}_{\text{Targeted Perturbation}} + \underbrace{\mathcal{L}_{pos}(\theta_\phi) + \lambda_2 \mathcal{L}_{sent}(\theta_\phi)}_{\text{Capability Preservation}} \right), \quad (5)$$

where $\rho > 0$ is a small hyperparameter that controls the neighborhood radius of the perturbation.

To efficiently solve the inner maximization in Eq. (5), we approximate the optimal perturbation ϵ^* using a first-order Taylor expansion. This simplifies the optimization to aligning with the gradient direction of the hallucination loss, thereby maximizing the likelihood of generating non-existent objects:

$$\begin{aligned} \epsilon^* &= \arg \max_{\|\epsilon\|_2 \leq \rho} \mathcal{L}_{neg}(\theta_\phi + \epsilon) \\ &\approx \rho \frac{\nabla_{\theta_\phi} \mathcal{L}_{neg}(\theta_\phi)}{\|\nabla_{\theta_\phi} \mathcal{L}_{neg}(\theta_\phi)\|_2}. \end{aligned} \quad (6)$$

This derivation reveals that the optimal perturbation ϵ^* serves as a directional indicator, pointing directly towards the region of highest vulnerability in the parameter space where the unlearned hallucinations are most liable to recur.

Substituting ϵ^* back into Eq. (5) transforms the inner maximization into a penalized objective:

$$\mathcal{L}_{neg}(\theta_\phi + \epsilon^*) \approx \mathcal{L}_{neg}(\theta_\phi) + \rho \|\nabla_{\theta_\phi} \mathcal{L}_{neg}(\theta_\phi)\|_2. \quad (7)$$

Here, the gradient norm term $\rho \|\nabla_{\theta_\phi} \mathcal{L}_{neg}\|_2$ functions as a sharpness regularizer. Minimizing this term explicitly flattens the loss landscape, reducing the model’s sensitivity to perturbations that would otherwise trigger hallucination relapse. However, directly minimizing Eq. (7) is computationally prohibitive as differentiating the norm term $\|\nabla \mathcal{L}_{neg}\|_2$ requires the Hessian matrix (second-order derivatives).

Efficient Gradient Approximation and Final Update. To minimize Eq. (7) efficiently without incurring the cost of Hessian computation, we leverage the first-order approximation strategy from SAM (Foret et al., 2020a). SAM demonstrates that the gradient of the sharpness-regularized objective can be effectively approximated by the gradient computed at the perturbed state $\theta_\phi + \epsilon^*$ (see Appendix B for the detailed derivation). Consequently, the final aggregated gradient g_{final} integrates two complementary signals: a robust suppression term computed at the worst-case perturbed state to penalize hallucination sensitivity, and standard preservation terms computed at the current parameter state to maintain general capabilities:

$$\begin{aligned} g_{final} &= \lambda_1 \nabla_{\theta_\phi} \mathcal{L}_{neg}(\theta_\phi + \epsilon^*) \\ &\quad + \nabla_{\theta_\phi} \mathcal{L}_{pos}(\theta_\phi) + \lambda_2 \nabla_{\theta_\phi} \mathcal{L}_{sent}(\theta_\phi). \end{aligned} \quad (8)$$

This optimization ensures that the erasure of hallucinations is not merely a superficial masking at a sharp point, but a robust removal stable within a neighborhood of parameters, thereby effectively defending against relearning attacks.

4 Experiments

4.1 Experimental Setup

Dataset. We conduct our experiments on the MSCOCO (Lin et al., 2014) dataset. We randomly sample 3,200 images, allocating 1,600 for validation and 1,600 for testing. For the unlearning process, the training set comprises approximately 30,000 triplets, where each training tuple consists of a negative caption, a positive caption, and a sentence-level preservation sample. Comprehensive data statistics and partitioning details are provided in Appendix A.1.

Metrics. To rigorously assess both hallucination mitigation and the preservation of model capabilities, we employ a comprehensive suite of metrics covering trustworthiness and helpfulness. **(1) Hallucination Evaluation:** We quantify object hallucinations using CHAIR (Rohrbach et al., 2018) for automated caption assessment, MHumanEval (Yu et al., 2023b) for human-verified judgment, and POPE (Fu et al., 2023) for discriminative hallucination assessment. **(2) Generation Quality Evaluation:** To ensure the unlearning process does not compromise linguistic quality, we calculate

Base Model	Method	Setting	Hallucination Rate					Generation Quality				
			Chair _S ↓	Chair _I ↓	Human _S ↓	Human _I ↓	POPE ↑	Bleu1 ↑	Bleu2 ↑	Bleu4 ↑	Info. ↑	ppl. ↓
LLaVA-v1.5-7B	None	Baseline	49.4	22.1	42.0	14.7	85.3	43.3	29.2	15.4	93.7	0.139
		Origin	41.8	18.3	24.0	7.7	85.9	47.1	32.7	18.2	93.5	0.113
	EFUF	w/ Relearn 60	45.8	19.7	26.0	10.4	85.3	45.8	31.5	17.3	93.5	0.111
		w/ Relearn 100	46.5	19.6	28.0	11.0	84.3	45.6	31.3	17.1	93.9	0.113
		w/ Relearn 140	48.9	20.9	29.0	11.8	84.0	45.2	30.9	16.7	93.7	0.114
		w/ LoRA FT	48.2	20.8	27.0	10.8	86.1	45.8	31.3	17.0	92.2	0.120
		w/ Adversarial	50.5	23.9	28.0	11.0	68.5	44.7	30.5	16.5	92.6	0.116
	SARE	Origin	34.4	14.7	21.0	6.5	86.7	48.0	33.5	18.9	92.1	0.101
		w/ Relearn 60	<u>34.6</u>	14.9	21.0	<u>6.7</u>	86.3	47.9	33.4	18.8	92.1	<u>0.098</u>
		w/ Relearn 100	35.4	15.3	<u>22.0</u>	7.9	86.2	<u>48.0</u>	33.4	18.8	92.0	<u>0.098</u>
		w/ Relearn 140	34.6	<u>14.8</u>	21.0	7.4	86.1	<u>48.0</u>	<u>33.5</u>	<u>18.9</u>	92.0	0.099
		w/ LoRA FT	37.9	17.4	24.0	9.5	<u>86.4</u>	46.4	31.9	17.6	91.2	0.084
		w/ Adversarial	39.9	17.8	24.0	9.8	67.7	48.5	<u>33.9</u>	19.2	92.4	0.104
mPLUG-Owl-7B	None	Baseline	69.6	33.5	60.0	24.1	85.6	43.3	29.1	15.1	91.1	0.129
		Origin	43.6	24.2	46.0	17.7	83.8	52.3	37.2	21.4	90.0	0.139
	EFUF	w/ Relearn 60	50.5	26.3	50.0	18.5	<u>84.8</u>	49.7	34.8	19.7	89.1	0.107
		w/ Relearn 100	55.2	28.6	52.0	18.9	82.1	47.7	33.1	18.4	89.9	0.107
		w/ Relearn 140	59.1	30.4	53.0	20.0	81.4	45.8	31.4	17.0	89.9	<u>0.106</u>
		w/ LoRA FT	58.6	29.7	52.0	20.3	82.0	47.5	32.6	18.0	89.5	0.107
		w/ Adversarial	50.0	26.9	48.0	18.5	74.0	52.2	37.1	21.3	89.9	0.112
	SARE	Origin	37.3	20.8	38.0	14.2	82.3	<u>53.5</u>	<u>38.2</u>	<u>22.2</u>	89.6	0.118
		w/ Relearn 60	42.3	21.8	40.0	16.3	<u>84.8</u>	51.2	36.3	20.8	89.6	0.110
		w/ Relearn 100	44.9	23.8	40.0	16.8	84.3	50.7	35.8	20.4	89.0	0.110
		w/ Relearn 140	45.8	23.9	42.0	17.7	84.0	49.9	35.1	19.9	88.4	0.108
		w/ LoRA FT	47.2	25.6	46.0	19.3	83.8	49.3	34.8	19.6	88.1	0.096
		w/ Adversarial	<u>37.5</u>	<u>21.2</u>	<u>39.0</u>	<u>14.7</u>	71.6	57.2	41.4	24.6	<u>90.1</u>	0.122

Table 1: Results on Hallucination Rates (Chair, Human, POPE) and Generation Quality (Bleu, Info., ppl.) under Relearning, LoRA, and Adversarial settings. “None” denotes the vanilla model. Bold and underlined indicate the best and second-best performance in each column.

BLEU (Papineni et al., 2002) scores for textual consistency, Informativeness for the semantic coverage of visual details, and Perplexity (PPL) to monitor text fluency. Detailed definitions and implementation specifics of these metrics are provided in Appendix A.2.

Models and Baselines. To demonstrate the universality and architectural adaptability of our approach, we conduct experiments on two representative MLLMs: mPLUG-Owl-7B (Ye et al., 2023) and LLaVA-v1.5-7B (Liu et al., 2023b,a). For each architecture, we compare three configurations: (1) the Vanilla model; (2) the EFUF baseline; and (3) our proposed SARE.

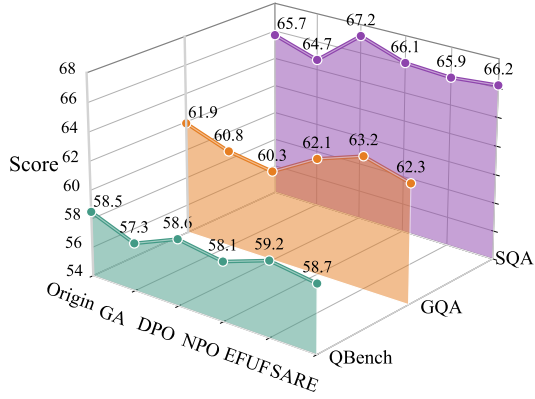
Experimental Settings. Adversarial configurations include: (1) **Relearning Attack**, where the unlearned model is fine-tuned on a subset of the original hallucination-inducing data to simulate memory recovery, monitoring the rebound across comprehensive evaluation metrics; (2) **LoRA Fine-tuning**, which examines the stability of the unlearning outcome by applying standard LoRA fine-tuning with approximately 10,000 samples from the original training dataset, testing if the hallucination suppression can be easily reactivated via parameter-efficient fine-tuning; and (3) **Adversarial Prompting**, which challenges the model with prompts that mandate exhaustive object listing to test its resistance against instruction-induced hallucinations. Prompt template for adversarial evaluation and additional implementation details are provided in Appendix C and Appendix A.3.

4.2 Main Results

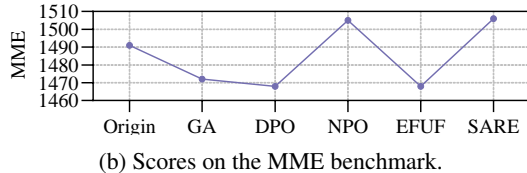
RQ1: Can SARE effectively erase hallucinations and maintain robustness against parameter-based attacks? Table 1 demonstrates the consistent superiority of SARE across diverse MLLM architectures. On mPLUG, our method achieves the most substantial reduction in hallucinations, slashing Chair_S from the baseline 69.6 to 37.3, a significant improvement over EFUF’s 43.6. It also maintains superior grounding, evidenced by the highest POPE score on LLaVA. Beyond static evaluation, SARE exhibits exceptional stability against parameter-based attacks. While EFUF suffers from catastrophic memory resurgence as relearning data increases, SARE maintains a much flatter performance curve; specifically, under Relearn 140 on LLaVA, SARE limits the Human_S rebound to 21.0 whereas EFUF surges to 29.0. Similarly, facing aggressive LoRA FT perturbations, SARE suppresses Chair_I to 17.4 on LLaVA, outperforming EFUF’s

Method	Hallucination Rate					Generation Quality				
	CHAIR _s ↓	CHAIR _i ↓	Hum _s ↓	Hum _i ↓	POPE ↑	Bleu-1 ↑	Bleu-2 ↑	Bleu-4 ↑	Info. ↑	ppl. ↓
LLaVA	49.4	22.1	42.0	14.7	85.3	43.3	29.2	15.4	93.7	0.139
+ f.g. unlearn.	46.1	21.8	44.0	13.9	80.0	43.4	29.2	15.5	92.3	0.143
+ Sent. Loss	37.8	19.7	40.0	12.7	70.0	45.9	31.7	17.5	91.8	0.087
SARE	34.4	14.7	21.0	6.5	86.7	48.0	33.5	18.9	92.1	0.101

Table 2: Ablation results on LLaVA across different unlearning granularities.



(a) Evaluation results on GQA, SQA, and QBench.



(b) Scores on the MME benchmark.

Figure 3: Assessment of General Capabilities on GQA, SQA, QBench, and MME. **SARE** effectively maintains foundational reasoning and comprehension.

20.8. Such broad resilience validates that Targeted-SAM anchors the model in a flat loss region, robustly withstanding significant weight shifts.

RQ2: Does SARE preserve general linguistic capabilities better than baselines? As presented in Table 1, we evaluate the generation quality using BLEU, Perplexity, and Informativeness metrics. For semantic fidelity, **SARE** achieves a Bleu-4 of 18.9 on LLaVA, surpassing EFUF’s 18.2 to demonstrate enhanced alignment without sacrificing coherence. Regarding fluency, **SARE** consistently outperforms EFUF by maintaining a PPL of 0.101 on LLaVA against the latter’s 0.113. Such superior fluency suggests that our optimization avoids linguistic degradation while enhancing text smoothness. Finally, Informativeness results confirm the preservation of semantic richness; on mPLUG-owl, **SARE** maintains a competitive 89.6, a value only 0.4 lower than EFUF, ensuring the model provides

detailed descriptions instead of evasive responses.

RQ3: Is the defense mechanism of SARE robust against perturbations? We further evaluate defense stability against input-level *Adversarial Prompting*. As shown in Table 1, EFUF exhibits significant vulnerability on LLaVA, where its Chair_S spikes to 50.5, nearly equivalent to the baseline. In contrast, **SARE** demonstrates robust resistance to such perturbations. On mPLUG, the disparity becomes particularly distinct as **SARE** maintains a low Chair_S of 37.5 while EFUF surges to 50.0. Such resilience confirms that our method transcends superficial pattern matching, fundamentally strengthening the model’s reliance on genuine visual evidence rather than spurious correlations.

4.3 Ablation Analysis

To investigate the individual contributions of each component in our framework, we conducted an ablation study on the LLaVA-v1.5-7B, comprehensively evaluating performance across both hallucination rates and generation quality. We compared four comparative settings: (1) **Origin**, representing the baseline LLaVA model; (2) **Fine-Grained Unlearning**, which exclusively employs the negative and positive subsentence datasets for targeted erasure and retention, excluding the sentence-level dataset; (3) **Sentence Loss Only**, which utilizes solely the sentence-level dataset for global consistency; and (4) **SARE**, the complete framework.

Effects of Fine-Grained Unlearning. As detailed in Table 2, applying fine-grained unlearning in isolation yields only marginal improvements in hallucination reduction. For instance, CHAIR_s decreases trivially from 49.4 to 46.1. However, these limited gains come at the cost of linguistic coherence. The decline in fluency is highlighted by the increased PPL and reduced informativeness. This suggests that myopic token-level suppression, without broader contextual constraints, disrupts the pre-trained language manifold.

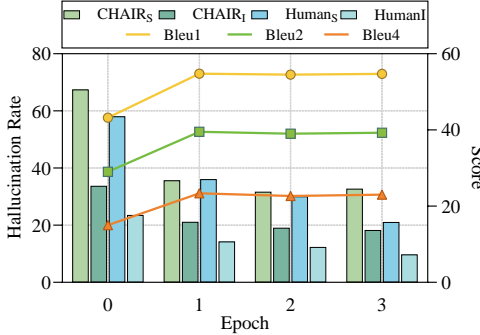


Figure 4: Training dynamics of **SARE**. Rapid convergence is achieved at Epoch 1, while further training leads to grounding collapse.

Effects of Sentence Loss. The Sentence Loss variant yields superior fluency with the lowest PPL of 0.087. While hallucination metrics appear to drop drastically, this improvement is deceptive. It correlates with a severe collapse in the POPE score from 85.3 to 70.0, indicating a failure in visual grounding. In this scenario, the model decouples visual inputs to generate safe but generic text, effectively sacrificing its fundamental visual recognition ability to satisfy the unlearning objective.

4.4 Reasoning and Comprehension Analysis

To holistically evaluate **SARE**, we measure its fine-grained reasoning, scientific understanding, and general perception across four benchmarks: MME (Fu et al., 2023), GQA (Hudson and Manning, 2019), ScienceQA (Lu et al., 2022), and QBench (Wang et al., 2023b). Figure 3 compares **SARE** against the baseline model and standard mitigation strategies, including GA (Jang et al., 2022b), DPO (Rafailov et al., 2023), NPO (Zhang et al., 2024a), and EFUF. **SARE** effectively maintains the model’s foundational capabilities across diverse benchmarks. Notably, it achieves a top MME score of 1506 and remains highly competitive across GQA, ScienceQA, and QBench. This confirms that **SARE** effectively mitigates hallucinations while maintaining robust reasoning capabilities.

4.5 Training Dynamics Analysis

We investigated training efficiency on mPLUG-Owl-7B. As illustrated in Figure 4, **SARE** exhibits rapid convergence, requiring only a single epoch to significantly reduce hallucinations and boost generation quality. Extending training beyond this point incurs unnecessary computational overhead while triggering a sharp POPE decline. This degradation renders the continued hallucination reduction

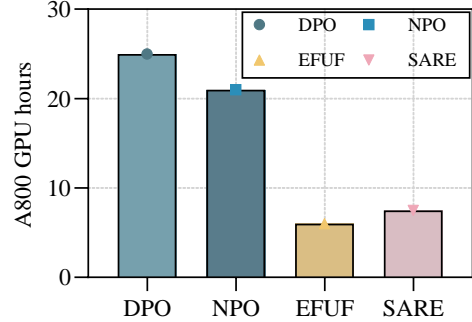


Figure 5: Efficiency comparison. **SARE** achieves significant speedup over DPO and NPO with competitive latency relative to EFUF.

meaningless, signaling a grounding collapse where the model sacrifices essential visual discrimination for superficial safety. Therefore, we select Epoch 1 as the optimal checkpoint, achieving a superior trade-off between erasure efficacy, visual grounding, and training costs.

4.6 Efficiency Analysis

We assessed the computational overhead of different methods using NVIDIA A800 GPUs. As reported in Figure 5, **SARE** demonstrates remarkable efficiency, achieving a significant speedup compared to computation-intensive baselines like DPO and NPO. While its latency is marginally higher than EFUF, **SARE** provides a superior trade-off by delivering substantially stronger hallucination mitigation with negligible additional cost.

4.7 More Experiments

To further substantiate the effectiveness of **SARE**, we provide extensive supplementary analyses in the appendix. Appendix D.1 evaluates generalizability to diverse MLLMs, while Appendix D.2 conducts sensitivity analyses on hyperparameters ρ , λ_1 and λ_2 . Qualitative case studies in Appendix E further demonstrate our robust resistance to relearning compared to standard unlearning.

5 Conclusion

In this paper, we reveal a critical robustness gap in MLLM hallucination unlearning, where standard methods converge to sharp local minima, leaving models vulnerable to rapid hallucination resurgence. Based on this insight, we introduce **SARE**, a sharpness-aware framework that enforces robust erasure through geometric regularization. By reformulating unlearning as a targeted min-max op-

timization, **SARE** simulates worst-case attacks during training to flatten the loss landscape, ensuring that hallucination suppression remains stable even under parameter shifts. Extensive experiments demonstrate that **SARE** effectively resists relearning and fine-tuning attacks while preserving foundational reasoning and linguistic capabilities.

Limitations

The limitations of our work reside in three primary aspects. First, the construction of the unlearning dataset relies on a static alignment-based filtering pipeline. While this efficiently identifies existing hallucinations, it cannot proactively capture latent hallucination triggers that are dormant in the pre-trained weights but might be activated under novel or out-of-distribution prompts. Second, although Targeted-SAM effectively flattens the loss landscape to ensure stability, it introduces a trade-off in optimization efficiency. The dual-step gradient computation doubles the training time per iteration, which may pose challenges for scaling to ultra-large datasets or real-time unlearning scenarios. Third, our robust erasure mechanism is currently optimized for object existence hallucinations where the visual evidence is explicit. The framework has yet to be extended to more nuanced hallucination types, such as incorrect object attributes or fallacious spatial positioning. Furthermore, applying this geometric regularization to abstract reasoning hallucinations, in which errors stem from fallacious logical chains instead of simple object misidentification, remains a significant future challenge.

Ethics Statement

Our research aims to enhance the reliability of Multimodal Large Language Models by mitigating hallucinations, which is a critical step toward ensuring the trustworthiness of AI systems in real-world applications. We identify and address three primary ethical considerations.

First, our methodology for data curation relies exclusively on publicly available datasets and automated alignment tools, ensuring that no private or sensitive user data is utilized during the unlearning process. Such an approach minimizes privacy risks while maintaining transparency in how hallucination patterns are identified and erased.

Second, we commit to releasing our code to the research community to foster collective defensive advancements and believe the net impact of this

research is strongly positive, offering a practical and principled step toward more reliable and trustworthy AI systems.

Finally, during drafting and revision, we used AI assistants to help optimize writing and improve clarity. No content was generated unsupervised or without verification.

References

Peter L. Bartlett, Philip M. Long, and Olivier Bousquet. 2022. [The dynamics of sharpness-aware minimization: Bouncing across ravines and drifting towards wide minima](#). *J. Mach. Learn. Res.*, 24:316:1–316:36.

Ali Furkan Biten, Lluís Gómez i Bigorda, and Dimosthenis Karatzas. 2021. [Let there be a clock on the beach: Reducing object hallucination in image captioning](#). *2022 IEEE/CVF Winter Conference on Applications of Computer Vision (WACV)*, pages 2473–2482.

Yinzhi Cao and Junfeng Yang. 2015. [Towards making systems forget with machine unlearning](#). *2015 IEEE Symposium on Security and Privacy*, pages 463–480.

Lin Chen, Jinsong Li, Xiao wen Dong, Pan Zhang, Conghui He, Jiaqi Wang, Feng Zhao, and Dahua Lin. 2023a. [Sharegpt4v: Improving large multi-modal models with better captions](#). In *European Conference on Computer Vision*.

Lin Chen, Jinsong Li, Xiao wen Dong, Pan Zhang, Conghui He, Jiaqi Wang, Feng Zhao, and Dahua Lin. 2023b. [Sharegpt4v: Improving large multi-modal models with better captions](#). In *European Conference on Computer Vision*.

Xiang Chen, Duanzheng Song, Honghao Gui, Chengxi Wang, Ningyu Zhang, Jiang Yong, Fei Huang, Chengfei Lv, Dan Zhang, and Huajun Chen. 2023c. [Factchd: Benchmarking fact-conflicting hallucination detection](#). *ArXiv*, abs/2310.12086.

Aghyad Deeb and Fabien Roger. 2024. [Do unlearning methods remove information from language model weights?](#) *ArXiv*, abs/2410.08827.

DeepSeek-AI and 1 others. 2024. [Deepseek-v3 technical report](#). *Preprint*, arXiv:2412.19437.

Jiawei Du, Hanshu Yan, Jiashi Feng, Joey Tianyi Zhou, Liangli Zhen, Rick Siow Mong Goh, and Vincent Y. F. Tan. 2021. [Efficient sharpness-aware minimization for improved training of neural networks](#). *ArXiv*, abs/2110.03141.

Chongyu Fan, Jinghan Jia, Yihua Zhang, Anil Ramakrishna, Mingyi Hong, and Sijia Liu. 2025. [Towards llm unlearning resilient to relearning attacks: A sharpness-aware minimization perspective and beyond](#). *ArXiv*, abs/2502.05374.

Pierre Foret, Ariel Kleiner, Hossein Mobahi, and Behnam Neyshabur. 2020a. **Sharpness-aware minimization for efficiently improving generalization**. *ArXiv*, abs/2010.01412.

Pierre Foret, Ariel Kleiner, Hossein Mobahi, and Behnam Neyshabur. 2020b. **Sharpness-aware minimization for efficiently improving generalization**. *ArXiv*, abs/2010.01412.

Chaoyou Fu, Peixian Chen, Yunhang Shen, Yulei Qin, Mengdan Zhang, Xu Lin, Zhenyu Qiu, Wei Lin, Jinrui Yang, Xiawu Zheng, Ke Li, Xing Sun, and Rongrong Ji. 2023. **Mme: A comprehensive evaluation benchmark for multimodal large language models**. *ArXiv*, abs/2306.13394.

Anish Gunjal, Jihan Yin, and Erhan Bas. 2023. **Detecting and preventing hallucinations in large vision language models**. In *AAAI Conference on Artificial Intelligence*.

Qidong Huang, Xiao wen Dong, Pan Zhang, Bin Wang, Conghui He, Jiaqi Wang, Dahua Lin, Weiming Zhang, and Neng H. Yu. 2023. **Opera: Alleviating hallucination in multi-modal large language models via over-trust penalty and retrospection-allocation**. *2024 IEEE/CVF Conference on Computer Vision and Pattern Recognition (CVPR)*, pages 13418–13427.

Drew A. Hudson and Christopher D. Manning. 2019. **Gqa: a new dataset for compositional question answering over real-world images**. *ArXiv*, abs/1902.09506.

Joel Jang, Dongkeun Yoon, Sohee Yang, Sungmin Cha, Moontae Lee, Lajanugen Logeswaran, and Minjoon Seo. 2022a. **Knowledge unlearning for mitigating privacy risks in language models**. In *Annual Meeting of the Association for Computational Linguistics*.

Joel Jang, Seonghyeon Yoon, Soochan Yang, Kyuhong Han, Seungone Han, Minjoon Ko, Seung-won Choi, and Minjoon Seo. 2022b. **Knowledge unlearning for generative language models**. In *Proceedings of the 2022 Conference on Empirical Methods in Natural Language Processing (EMNLP)*, pages 3458–3472.

Ziwei Ji, Nayeon Lee, Rita Frieske, Tiezheng Yu, Dan Su, Yan Xu, Etsuko Ishii, Yejin Bang, Delong Chen, Wenliang Dai, Andrea Madotto, and Pascale Fung. 2022. **Survey of hallucination in natural language generation**. *ACM Computing Surveys*, 55:1 – 38.

Jungmin Kwon, Jeongseop Kim, Hyunseong Park, and Inae Choi. 2021. **Asam: Adaptive sharpness-aware minimization for scale-invariant learning of deep neural networks**. *ArXiv*, abs/2102.11600.

Zhengfeng Lai, Vasileios Saveris, Chen Chen, Hong-You Chen, Haotian Zhang, Bowen Zhang, Juan Lao Tebar, Wenze Hu, Zhe Gan, Peter Grasch, Meng Cao, and Yinfei Yang. 2024. **Revisit large-scale image-caption data in pre-training multimodal foundation models**. *ArXiv*, abs/2410.02740.

Bo Li, Yuanhan Zhang, Liangyu Chen, Jinghao Wang, Jingkang Yang, and Ziwei Liu. 2023a. **Otter: A multi-modal model with in-context instruction tuning**. *IEEE Transactions on Pattern Analysis and Machine Intelligence*, 47:7543–7557.

Bo Li, Yuanhan Zhang, Liangyu Chen, Jinghao Wang, Jingkang Yang, and Ziwei Liu. 2023b. **Otter: A multi-modal model with in-context instruction tuning**. *IEEE Transactions on Pattern Analysis and Machine Intelligence*, 47:7543–7557.

Yifan Li, Yifan Du, Kun Zhou, Jinpeng Wang, Wayne Xin Zhao, and Ji rong Wen. 2023c. **Evaluating object hallucination in large vision-language models**. In *Conference on Empirical Methods in Natural Language Processing*.

Tsung-Yi Lin, Michael Maire, Serge J. Belongie, James Hays, Pietro Perona, Deva Ramanan, Piotr Dollár, and C. Lawrence Zitnick. 2014. **Microsoft coco: Common objects in context**. In *European Conference on Computer Vision*.

Fuxiao Liu, Kevin Lin, Linjie Li, Jianfeng Wang, Yaser Yacoob, and Lijuan Wang. 2023a. **Mitigating hallucination in large multi-modal models via robust instruction tuning**. In *International Conference on Learning Representations*.

Hanchao Liu, Wenyuan Xue, Yifei Chen, Dapeng Chen, Xiutian Zhao, Ke Wang, Liping Hou, Rong-Zhi Li, and Wei Peng. 2024a. **A survey on hallucination in large vision-language models**. *ArXiv*, abs/2402.00253.

Haotian Liu, Chunyuan Li, Qingyang Wu, and Yong Jae Lee. 2023b. **Visual instruction tuning**. *ArXiv*, abs/2304.08485.

Yujian Liu, Yang Zhang, T. Jaakkola, and Shiyu Chang. 2024b. **Revisiting who's harry potter: Towards targeted unlearning from a causal intervention perspective**. In *Conference on Empirical Methods in Natural Language Processing*.

Pan Lu, Swaroop Mishra, Tony Xia, Liang Qiu, Kai-Wei Chang, Song-Chun Zhu, Oyvind Tafjord, Peter Clark, and A. Kalyan. 2022. **Learn to explain: Multimodal reasoning via thought chains for science question answering**. *ArXiv*, abs/2209.09513.

Aengus Lynch, Phillip Guo, Aidan Ewart, Stephen Casper, and Dylan Hadfield-Menell. 2024. **Eight methods to evaluate robust unlearning in llms**. *ArXiv*, abs/2402.16835.

Kishore Papineni, Salim Roukos, Todd Ward, and Wei Jing Zhu. 2002. **Bleu: a method for automatic evaluation of machine translation**. In *Proceedings of the 40th Annual Meeting on Association for Computational Linguistics, ACL '02*, page 311–318, USA. Association for Computational Linguistics.

Adam Paszke, Sam Gross, Francisco Massa, Adam Lerer, James Bradbury, Gregory Chanan, Trevor Killeen, Zeming Lin, Natalia Gimelshein, Luca Antiga, Alban Desmaison, Andreas Köpf, Edward Yang, Zachary DeVito, Martin Raison, Alykhan Tejani, Sasank Chilamkurthy, Benoit Steiner, Lu Fang, and 2 others. 2019. *Pytorch: An imperative style, high-performance deep learning library*. *ArXiv*, abs/1912.01703.

Alec Radford, Jeffrey Wu, Rewon Child, David Luan, Dario Amodei, and Ilya Sutskever. 2019. Language models are unsupervised multitask learners. *OpenAI blog*, 1(8):9.

Rafael Rafailov, Archit Sharma, Eric Mitchell, Christopher D. Manning, Stefano Ermon, and Chelsea Finn. 2023. *Direct preference optimization: Your language model is secretly a reward model*. In *Advances in Neural Information Processing Systems 36: Annual Conference on Neural Information Processing Systems 2023, NeurIPS 2023, New Orleans, LA, USA, December 10 - 16, 2023*.

Anna Rohrbach, Lisa Anne Hendricks, Kaylee Burns, Trevor Darrell, and Kate Saenko. 2018. *Object hallucination in image captioning*. In *Proceedings of the 2018 Conference on Empirical Methods in Natural Language Processing*, pages 4035–4045, Brussels, Belgium. Association for Computational Linguistics.

Shubhankar Singh, Purvi Chaurasia, Yerram Varun, Pranshu Pandya, Vatsal Gupta, Vivek Gupta, and Dan Roth. 2024. *Flowvqa: Mapping multimodal logic in visual question answering with flowcharts*. *ArXiv*, abs/2406.19237.

Zhiqing Sun, Sheng Shen, Shengcao Cao, Haotian Liu, Chunyuan Li, Yikang Shen, Chuang Gan, Liangyan Gui, Yu-Xiong Wang, Yiming Yang, Kurt Keutzer, and Trevor Darrell. 2023. *Aligning large multimodal models with factually augmented rlhf*. *ArXiv*, abs/2309.14525.

Szilvia Ujv'ary, Zsigmond Telek, Anna Kerekes, Anna M'esz'aros, and Ferenc Husz'ar. 2022. *Rethinking sharpness-aware minimization as variational inference*. *ArXiv*, abs/2210.10452.

Enayat Ullah, Tung Mai, Anup B. Rao, Ryan A. Rossi, and R. Arora. 2021. *Machine unlearning via algorithmic stability*. In *Annual Conference Computational Learning Theory*.

Bin Wang, Fan Wu, Xiao Han, Jiahui Peng, Huaping Zhong, Pan Zhang, Xiao wen Dong, Weijia Li, Wei Li, Jiaqi Wang, and Conghui He. 2023a. *Vigc: Visual instruction generation and correction*. In *AAAI Conference on Artificial Intelligence*.

Bin Wang, Fan Wu, Xiao Han, Jiahui Peng, Huaping Zhong, Pan Zhang, Xiao wen Dong, Weijia Li, Wei Li, Jiaqi Wang, and Conghui He. 2023b. *Vigc: Visual instruction generation and correction*. In *AAAI Conference on Artificial Intelligence*.

Jianfeng Wang, Zhengyuan Yang, Xiaowei Hu, Linjie Li, Kevin Lin, Zhe Gan, Zicheng Liu, Ce Liu, and Lijuan Wang. 2022a. *Git: A generative image-to-text transformer for vision and language*. *ArXiv*, abs/2205.14100.

Jianfeng Wang, Zhengyuan Yang, Xiaowei Hu, Linjie Li, Kevin Lin, Zhe Gan, Zicheng Liu, Ce Liu, and Lijuan Wang. 2022b. *Git: A generative image-to-text transformer for vision and language*. *ArXiv*, abs/2205.14100.

Zeming Wei, Jingyu Zhu, and Yihao Zhang. 2023. *Sharpness-aware minimization alone can improve adversarial robustness*. In *ICML 2023 Workshop on New Frontiers in Adversarial Machine Learning*.

Shangyu Xing, Fei Zhao, Zhen Wu, Tuo An, Weihao Chen, Chunhui Li, Jianbing Zhang, and Xinyu Dai. 2024. *Efuf: Efficient fine-grained unlearning framework for mitigating hallucinations in multimodal large language models*. *ArXiv*, abs/2402.09801.

Qinghao Ye, Haiyang Xu, Guohai Xu, Jiabo Ye, Ming Yan, Yi Zhou, Junyan Wang, Anwen Hu, Pengcheng Shi, Yaya Shi, Chenliang Li, Yuanhong Xu, Hehong Chen, Junfeng Tian, Qiang Qi, Ji Zhang, and Feiyan Huang. 2023. *mplug-owl: Modularization empowers large language models with multimodality*. *ArXiv*, abs/2304.14178.

Shukang Yin, Chaoyou Fu, Sirui Zhao, Tong Xu, Hao Wang, Dianbo Sui, Yunhang Shen, Ke Li, Xingguo Sun, and Enhong Chen. 2023. *Woodpecker: hallucination correction for multimodal large language models*. *Science China Information Sciences*, 67.

Haoxuan You, Haotian Zhang, Zhe Gan, Xianzhi Du, Bowen Zhang, Zirui Wang, Liangliang Cao, Shih-Fu Chang, and Yinfei Yang. 2023. *Ferret: Refer and ground anything anywhere at any granularity*. *ArXiv*, abs/2310.07704.

Tianyu Yu, Yuan Yao, Haoye Zhang, Taiwen He, Yifeng Han, Ganqu Cui, Jinyi Hu, Zhiyuan Liu, Hai-Tao Zheng, Maosong Sun, and Tat-Seng Chua. 2023a. *Rlfh-v: Towards trustworthy mllms via behavior alignment from fine-grained correctional human feedback*. In *2024 IEEE/CVF Conference on Computer Vision and Pattern Recognition (CVPR)*, pages 13807–13816.

Tianyu Yu, Yuan Yao, Haoye Zhang, Taiwen He, Yifeng Han, Ganqu Cui, Jinyi Hu, Zhiyuan Liu, Hai-Tao Zheng, Maosong Sun, and Tat-Seng Chua. 2023b. *Rlfh-v: Towards trustworthy mllms via behavior alignment from fine-grained correctional human feedback*. In *2024 IEEE/CVF Conference on Computer Vision and Pattern Recognition (CVPR)*, pages 13807–13816.

Ruiqi Zhang, Licong Lin, Yu Bai, and Song Mei. 2024a. *Negative preference optimization: From catastrophic collapse to effective unlearning*. *ArXiv*, abs/2404.05868.

Yihao Zhang, Hangzhou He, Jingyu Zhu, Huanran Chen, Yifei Wang, and Zeming Wei. 2024b. [On the duality between sharpness-aware minimization and adversarial training](#). *ArXiv*, abs/2402.15152.

Yue Zhang, Yafu Li, Leyang Cui, Deng Cai, Lemao Liu, Tingchen Fu, Xinting Huang, Enbo Zhao, Yu Zhang, Yulong Chen, Longyue Wang, Anh Tuan Luu, Wei Bi, Freda Shi, and Shuming Shi. 2023. [Siren’s song in the ai ocean: A survey on hallucination in large language models](#). *ArXiv*, abs/2309.01219.

Fei Zhao, Taotian Pang, Chunhui Li, Zhen Wu, Junjie Guo, Shangyu Xing, and Xinyu Dai. 2024. [Aligngpt: Multi-modal large language models with adaptive alignment capability](#). *ArXiv*, abs/2405.14129.

Zhiyuan Zhao, Bin Wang, Linke Ouyang, Xiao wen Dong, Jiaqi Wang, and Conghui He. 2023. [Beyond hallucinations: Enhancing l4lms through hallucination-aware direct preference optimization](#). *ArXiv*, abs/2311.16839.

Deyao Zhu, Jun Chen, Xiaoqian Shen, Xiang Li, and Mohamed Elhoseiny. 2023. [Minigpt-4: Enhancing vision-language understanding with advanced large language models](#). *ArXiv*, abs/2304.10592.

Lanyun Zhu, Deyi Ji, Tianrun Chen, Peng Xu, Jieping Ye, and Jun Liu. 2024. [Ibd: Alleviating hallucinations in large vision-language models via image-biased decoding](#). *2025 IEEE/CVF Conference on Computer Vision and Pattern Recognition Workshops (CVPRW)*, pages 1615–1624.

A Detailed Experimental Setups

A.1 Dataset

We utilize the MSCOCO 2014 dataset (Lin et al., 2014) as our primary source, following the data construction protocol established in EFUF (Xing et al., 2024). To ensure a rigorous evaluation, we randomly reserve 3,200 images that are strictly excluded from the training process, allocating 1,600 images for validation and another 1,600 images for testing. The remaining images serve as the candidate pool for constructing our unlearning dataset. Unlike traditional supervised fine-tuning, our approach does not utilize ground-truth captions during training. Since our approach necessitates only the raw images and their associated text queries, the official annotations provided by MSCOCO are used exclusively for evaluation purposes. From the candidate pool, approximately 30,000 training samples are curated via a CLIP-based filtering strategy with empirical thresholds (T_0, T_1, T_2). These samples are distributed among positive subsentences (D_{pos}), negative subsentences (D_{neg}), and sentence-level retention data (D_{sent}).

A.2 Metrics

Metrics on Hallucination Evaluation To quantify the degree of hallucination, we employ three metrics: CHAIR(automated caption assessment), MHumanEval(human-verified judgment) and POPE(visual perception capabilities).

- **CHAIR.** Caption Hallucination Assessment with Image Relevance (CHAIR) (Rohrbach et al., 2018) is a widely used image captioning metric that identifies hallucinated objects by comparing the extracted objects with ground truth labels and evaluates both at the instance level ($CHAIR_I$) and sentence level ($CHAIR_S$). Below are the detailed formation of these two metrics.

$$CHAIR_I = \frac{|\{\text{hallucinated objects}\}|}{|\{\text{all mentioned objects}\}|} \quad (9)$$

$$CHAIR_S = \frac{|\{\text{hallucinated captions}\}|}{|\{\text{total captions}\}|} \quad (10)$$

where a "hallucinated caption" is defined as any response containing at least one object not present in the ground truth.

- **MHumanEval.** (Yu et al., 2023b) Given the open-ended generation capabilities of MLLMs, the standard CHAIR metric faces limitations as it relies on MSCOCO annotations which only cover a restricted set of pre-defined object categories, inevitably causing inaccuracies in evaluation. To address this, we incorporate human judgment into our evaluation. Following (Yu et al., 2023a), we conduct a manual audit on a randomly sampled set of 100 generated captions. To ensure comparability with the CHAIR metric, we compute human-verified hallucination rates at both the instance and sentence granularities, providing a rigorous measurement of model reliability beyond the constraints of fixed vocabularies.

- **POPE.** (Fu et al., 2023) The Polling-based Object Probing Evaluation (POPE) (Fu et al., 2023) is a VQA-based evaluation protocol designed to probe the model’s visual perception stability. It queries the model with simple "Yes/No" questions regarding the existence of specific objects in the image. To prevent the model from exploiting statistical biases, POPE employs three sampling settings: Random (randomly sampling non-existent objects), Popular (sampling frequent but non-existent objects), and Adversarial (sampling co-occurring but non-existent objects). We report the F1 score for performance evaluation.

Metrics on Generation Quality Evaluation While the primary objective of our method is to mitigate hallucinations, it is equally critical to ensure that the unlearning process does not degrade the model’s general linguistic capabilities. We employ three distinct metrics to evaluate the consistency, utility and fluency of the generated content.

- **BLEU.** To measure the lexical alignment between the generated captions and human-written references, we utilize the BLEU metric (Papineni et al., 2002). BLEU calculates the precision of n-gram overlaps, serving as a standard proxy for linguistic consistency. While less sensitive to semantics than LLM-based metrics, it remains a vital benchmark for ensuring that the unlearning process does not catastrophically alter the model’s vocabulary usage or sentence structure.

- **Informativeness.** Standard lexical metrics often fail to gauge whether key visual con-

cepts are preserved. To address this, we implement a Semantic Coverage Score utilizing DeepSeek (DeepSeek-AI et al., 2024) as an external judge. Instead of simple text matching, we prompt the evaluator to analyze the semantic alignment between the model’s response and the ground-truth captions. This metric specifically quantifies the recall of essential visual details present in the reference, serving as a high-level proxy for model utility.

- **Perplexity.** To quantify the linguistic naturalness and coherence of the generated captions, we compute Perplexity (ppl.) using an external pre-trained GPT-2 model (Radford et al., 2019). Mathematically, this metric represents the exponentiated average negative log-likelihood of the generated token sequence. A lower PPL score indicates that the output is statistically closer to the distribution of natural human language, serving as a critical indicator that our unlearning intervention has not compromised the fundamental language modeling capabilities of the MLLM.

A.3 Implementation Details

We implement all models using the PyTorch framework (Paszke et al., 2019) and conduct experiments on an NVIDIA A800 GPU. During unlearning, we only tune the multimodal mapping layers of each MLLM to maintain architectural integrity. All models are trained for a fixed 1 epoch using the AdamW optimizer with a learning rate η of 1e-5 and weight decay of 0.05. For our SAREframework, the unlearning loss weight λ_1 and sentence loss weight λ_2 are set to 0.3 and 0.2, respectively, while the perturbation radius ρ is set to 0.05. Regarding the data curation pipeline described in Sec. 3.3, the thresholds for visual anchors (T_0) and hallucinated targets (T_1) are established at 32 and 23. Furthermore, to balance the sample distribution between sentence-level and subsentence-level data, the reliability threshold (T_2) for the sentence-level dataset D_{sent} is set to 27.5.

B Derivation of Gradient Approximation

In this section, we provide the detailed mathematical justification for approximating the explicit Hessian computation with a second forward-backward pass. Since the retention losses are independent of the perturbation ϵ , we focus our analysis exclusively on the hallucination component. In this

context, the Targeted-SAM objective effectively minimizes a regularized loss defined as:

$$\mathcal{J}_{neg}(\theta_\phi) = \mathcal{L}_{neg}(\theta_\phi) + \rho \|\nabla_{\theta_\phi} \mathcal{L}_{neg}(\theta_\phi)\|_2. \quad (11)$$

To update the parameters, we require the gradient of this objective with respect to θ_ϕ .

First, we analyze the derivative of the gradient norm regularization term $\rho \|\nabla_{\theta_\phi} \mathcal{L}_{neg}(\theta_\phi)\|_2$. Let $g = \nabla_{\theta_\phi} \mathcal{L}_{neg}(\theta_\phi)$ denote the gradient vector. The gradient of its L_2 norm is derived using the chain rule:

$$\begin{aligned} \nabla_{\theta_\phi} \|g\|_2 &= \nabla_{\theta_\phi} (g^\top g)^{1/2} \\ &= \frac{1}{2(g^\top g)^{1/2}} \cdot \nabla_{\theta_\phi} (g^\top g) \\ &= \frac{1}{2\|g\|_2} \cdot (2\mathbf{H}g) \\ &= \frac{\mathbf{H}\nabla_{\theta_\phi} \mathcal{L}_{neg}(\theta_\phi)}{\|\nabla_{\theta_\phi} \mathcal{L}_{neg}(\theta_\phi)\|_2}, \end{aligned} \quad (12)$$

where $\mathbf{H} = \nabla_{\theta_\phi}^2 \mathcal{L}_{neg}(\theta_\phi)$ is the Hessian matrix, and we utilize the property $\nabla_{\theta_\phi} (g^\top g) = 2\mathbf{H}g$.

Substituting this result back into the gradient of the total objective \mathcal{J}_{neg} , the **theoretical gradient** is derived as:

$$\begin{aligned} \nabla_{\theta_\phi} \mathcal{J}_{neg} &= \nabla_{\theta_\phi} \mathcal{L}_{neg}(\theta_\phi) \\ &\quad + \rho \frac{\mathbf{H}\nabla_{\theta_\phi} \mathcal{L}_{neg}(\theta_\phi)}{\|\nabla_{\theta_\phi} \mathcal{L}_{neg}(\theta_\phi)\|_2}. \end{aligned} \quad (13)$$

This confirms that the exact update direction explicitly involves the Hessian-vector product $\mathbf{H}v$, where v is the normalized gradient direction.

Directly computing $\mathbf{H}v$ is computationally prohibitive. However, we demonstrate that this term naturally arises from the gradient at the perturbed state. Consider the gradient computed at $\theta_\phi + \epsilon^*$, where $\epsilon^* = \rho \frac{\nabla_{\theta_\phi} \mathcal{L}_{neg}(\theta_\phi)}{\|\nabla_{\theta_\phi} \mathcal{L}_{neg}(\theta_\phi)\|_2}$. We apply a first-order Taylor expansion to the gradient function $\nabla_{\theta_\phi} \mathcal{L}_{neg}(\cdot)$ around θ_ϕ :

$$\begin{aligned} &\nabla_{\theta_\phi} \mathcal{L}_{neg}(\theta_\phi + \epsilon^*) \\ &\approx \nabla_{\theta_\phi} \mathcal{L}_{neg}(\theta_\phi) + \mathbf{H}\epsilon^* \\ &= \nabla_{\theta_\phi} \mathcal{L}_{neg}(\theta_\phi) + \mathbf{H} \left(\rho \frac{\nabla_{\theta_\phi} \mathcal{L}_{neg}(\theta_\phi)}{\|\nabla_{\theta_\phi} \mathcal{L}_{neg}(\theta_\phi)\|_2} \right) \\ &= \nabla_{\theta_\phi} \mathcal{L}_{neg}(\theta_\phi) + \rho \frac{\mathbf{H}\nabla_{\theta_\phi} \mathcal{L}_{neg}(\theta_\phi)}{\|\nabla_{\theta_\phi} \mathcal{L}_{neg}(\theta_\phi)\|_2}. \end{aligned} \quad (14)$$

Comparing Eq. (13) and Eq. (14), we observe that the gradient computed at the perturbed state serves

as a first-order approximation to the theoretical SAM gradient. This proves that our approach implicitly captures the curvature information required for robust optimization, effectively bypassing the computationally expensive materialization of the Hessian matrix.

C Prompt Templates for Adversarial Evaluation

Adversarial prompt

Please provide a comprehensive description of the image. Systematically list all the clearly identifiable objects you see, ensuring you do not overlook any distinct items.

D More Experiments

D.1 Generalizability Analysis

To demonstrate the versatility and model-agnostic nature of our proposed framework, we extend our evaluation to two other representative Multimodal Large Language Models (MLLMs): MiniGPT-4 (Zhu et al., 2023) and ShareGPT4V (Chen et al., 2023b). As summarized in Table 3, our framework exhibits robust generalizability across diverse architectures, consistently surpassing both the original models and the EFUF baseline.

Notably, results on MiniGPT-4 reveal a significant deviation from the typical trade-off between unlearning efficacy and model utility. While standard unlearning often compromises general capabilities, our method achieves superior linguistic fluency compared to the original model. This indicates that our targeted sharpness tuning operates with high precision: by flattening the loss landscape, it effectively prunes specific hallucination patterns and refines the model’s probability distribution, rather than indiscriminately damaging its knowledge base.

This architectural robustness is further corroborated on ShareGPT4V, where **SARE** establishes comprehensive superiority across both safety and generation quality metrics. These results confirm that the erasure of hallucinations is not merely a superficial suppression, but a stable optimization that preserves, and in some instances enhances, the fundamental generative capabilities of the MLLM.

D.2 Hyperparameter Sensitivity Analysis

In this segment, we delve into the effects of varying three critical hyperparameters: the negative loss weight λ_1 , the sentence-level preservation weight λ_2 , and the perturbation radius ρ . Our investigation, conducted on the LLaVA-v1.5-7B model, aims to understand how adjustments in these parameters influence the delicate trade-off between suppressing hallucinations and maintaining generation quality. The empirical results are summarized in Table 4.

- **Impact of Negative Loss Weight λ_1 .** The coefficient λ_1 governs the magnitude of the penalty applied to hallucinated samples. As λ_1 increases from 0.1 to 0.3, we observe significant improvements in both hallucination reduction and generation quality, suggesting that a sufficient penalty is requisite to push the model out of hallucination-prone regions. However, a further increase to 0.4 triggers a sharp degradation across all metrics (e.g., PPL rises to 0.126). This performance drop likely stems from **distribution collapse**: an excessively aggressive unlearning penalty disrupts the model’s linguistic manifold, forcing the probability mass to shift unpredictably. This destabilizes the optimization, causing both catastrophic forgetting of valid knowledge and a resurgence of hallucinations due to the broken probability distribution. Consequently, $\lambda_1 = 0.3$ is identified as the optimal balance point.
- **Impact of Sentence Loss Weight λ_2 .** The coefficient λ_2 regulates the importance of the sentence-level objective, serving as an anchor to preserve capabilities. While a moderate λ_2 (0.3) acts as a necessary stabilizer, increasing it to 0.4 results in a global performance decline—hallucination rates rise, and generation quality deteriorates (e.g., Bleu-1 drops and PPL worsens). We attribute this to **over-regularization and gradient conflict**. An overly dominant λ_2 imposes rigid constraints that conflict with the gradient updates required for unlearning (L_{neg}) and visual alignment (L_{pos}). This high tension prevents the model from converging to an optimal solution, trapping it in a suboptimal state where neither visual grounding nor linguistic fluency is effectively maintained. Thus, $\lambda_2 = 0.3$ is selected as the optimal setting.

Model	Method	Hallucination Rate			Generation Quality				
		CHAIR _S ↓	CHAIR _I ↓	POPE ↑	Bleu-1 ↑	Bleu-2 ↑	Bleu-4 ↑	Info. ↑	PPL ↓
MiniGPT-4	Original	45.9	23.2	81.0	43.8	29.5	15.5	86.7	0.134
	EFUF	38.9	21.1	82.3	45.6	31.1	16.7	87.5	0.121
	Ours	35.4	18.8	81.3	48.1	32.8	17.2	85.1	0.110
ShareGPT4V	Original	46.8	22.3	87.8	43.3	29.2	15.4	89.6	0.157
	EFUF	36.9	18.4	88.1	46.9	32.5	18.1	91.1	0.159
	Ours	34.7	14.9	91.0	47.9	33.4	18.8	92.0	0.112

Table 3: Performance comparison on generalizability. We compare the original models with the EFUF baseline and our proposed method on MiniGPT-4 and ShareGPT4V benchmarks. **Bold** denotes the best performance.

Parameter	Value	Hallucination Rate					Generation Quality				
		Chair _S ↓	Chair _I ↓	Human _S ↓	Human _I ↓	POPE ↑	Bleu1 ↑	Bleu2 ↑	Bleu4 ↑	Info. ↑	ppl. ↓
λ_1	0.1	49.0	21.9	40.0	14.1	87.9	43.6	29.5	15.6	92.8	0.125
	0.2	30.2	14.6	18.0	6.3	73.4	47.6	33.1	18.6	92.3	0.100
	0.3	29.1	13.6	18.0	6.1	85.9	47.7	33.2	18.7	92.3	0.101
	0.4	50.4	22.4	42.0	14.0	89.3	43.6	29.4	15.6	92.6	0.126
λ_2	0.1	50.4	22.4	42.0	13.7	90.0	43.5	29.4	15.5	92.9	0.125
	0.2	46.1	20.2	38.0	11.3	79.7	44.6	30.3	16.3	92.5	0.110
	0.3	29.1	13.6	18.0	6.1	85.9	47.7	33.2	18.7	92.3	0.101
	0.4	43.8	21.7	35.0	12.7	79.6	43.7	29.6	15.7	92.6	0.115
ρ	0.01	44.0	21.2	35.0	11.8	70.0	43.7	29.6	15.8	93.1	0.100
	0.05	29.1	13.6	18.0	6.1	85.9	47.7	33.2	18.7	92.3	0.101
	0.10	29.5	14.0	19.0	6.8	70.6	47.7	33.2	18.6	92.0	0.101
	0.15	50.2	22.1	41.0	13.0	89.2	43.6	29.4	15.6	93.3	0.125

Table 4: Hyperparameter Sensitivity Analysis on LLaVA-v1.5-7B. We investigate the impact of the negative loss weight λ_1 , the sentence loss weight λ_2 , and the perturbation radius ρ . The best configuration is highlighted in bold.

- **Impact of Perturbation Radius ρ .** The perturbation parameter ρ controls the magnitude of the worst-case noise injected during optimization. When ρ is small (0.01), the method yields limited gains, behaving similarly to standard fine-tuning. Increasing ρ to 0.05 significantly enhances performance, confirming that an appropriate level of perturbation effectively flattens the loss landscape. Notably, performance degrades drastically when ρ exceeds 0.10 (reaching 0.15). This drop suggests that an overly large perturbation radius pushes the model parameters too far from the optimal manifold, making it difficult for the outer minimization step to recover a valid solution. Based on these observations, we adopt $\rho = 0.05$ as the default configuration.

E Case Study

To provide a more intuitive understanding of how **SARE** resists hallucination resurgence, we present qualitative comparisons between standard unlearning and our method under relearning attacks.



Prompt: Please describe this image in great detail. Your response should have at least 100 words.

Standard Unlearning Output: The image depicts a woman standing in a kitchen, preparing food on a stove. She is wearing a plaid shirt and a pink head scarf. The kitchen is equipped with two stoves, one on the left side and another on the right side of the room. There are several bottles placed around the kitchen, some on the countertops and others on the shelves. Additionally, there are two bowls in the scene, one on the left side and another on the right side of the kitchen.

TRUST Output: In the image, a woman is standing in a kitchen preparing food. She is wearing a plaid shirt and a pink head scarf, and she appears to be smiling as she cooks. The kitchen is equipped with two stoves, one on the left side and another on the right side of the room. There are two pans on the stoves, one on the left and another on the right.

Relearning Attack

Prompt: Please describe this image in great detail. Your response should have at least 100 words.

Standard Unlearning Output: The image depicts a woman standing in a kitchen, preparing food on a stove. She is wearing a plaid shirt and a pink headscarf. There are several pots and pans on the stove, indicating that she is cooking a variety of dishes. In addition to the stove, there are multiple bottles scattered around the kitchen, possibly containing ingredients or cooking oils. **A chair is also present in the scene, placed near the stove. Another person can be seen in the background, but they are not the main focus of the image.**

TRUST Output: The image depicts a woman standing in a kitchen, preparing food on a stove. She is wearing a pink head scarf and appears to be smiling while cooking. The kitchen is equipped with two stoves, one on the left side and another on the right side of the woman. In addition to the stoves, there are several bottles placed around the kitchen, some on the countertops and others on the floor. There are also two bowls in the kitchen, one on the left side and another on the right side of the woman.



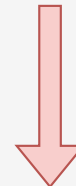
Figure 6: Qualitative comparisons demonstrating the superior robustness of SARE against relearning attacks in contrast to standard unlearning. The red text denotes specific hallucinated content, while the orange indicates sentences containing hallucinations.

Prompt: Please describe this image in great detail. Your response should have at least 100 words.

Standard Unlearning Output: The image depicts a train station with two trains parked side by side on the tracks. The first train is on the left side of the image, and the second train is on the right side. The train on the left appears to be a passenger train, while the train on the right appears to be a freight train.



TRUST Output: The image depicts a train station with two trains on the tracks. One train is positioned on the left side of the image, and the other train is on the right side. The train on the left appears to be a passenger train, while the train on the right is a freight train.



Relearning Attack

Prompt: Please describe this image in great detail. Your response should have at least 100 words.

Standard Unlearning Output: The image depicts a train station with two trains parked on the tracks. One train is positioned on the left side of the image, while the other is on the right side. The train on the left appears to be a passenger train, while the train on the right is a freight train. There are a few people in the scene, with one person standing close to the left train and two others near the right train. Additionally, there is a handbag located near the person standing close to the left train.



TRUST Output: The image depicts a train station with two trains on the tracks. One train is positioned on the left side of the image, and the other train is on the right side. The train on the left appears to be a passenger train, while the train on the right appears to be a freight train.

Figure 7: Qualitative comparisons demonstrating the superior robustness of SARE against relearning attacks in contrast to standard unlearning. The red text denotes specific hallucinated content, while the orange indicates sentences containing hallucinations.